Journal of Materials Chemistry C

Accepted Manuscript

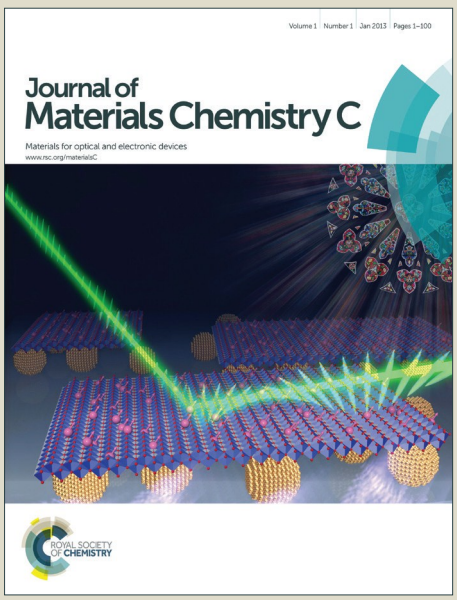

ROYAL SOCIETY OF CHEMISTRY

www.rsc.org/materialsC

Effects of the Benzoxazole Group on Green Fluorescent Protein Chromophore Crystal Structure and Solid State Photophysics

Abdelhamid Ghodbane,[ab#] W. Brett Fellows,[c#] John R. Bright,[cd] Debashree Ghosh,[e] Nathalie Saffon,[f] Laren M. Tolbert,[c] Suzanne Fery-Forgues,[gh*] and Kyril M. Solntsev [ci*]

[a] CNRS, Université de Toulouse, ITAV-USR 3505, F31106 Toulouse, France

[b] CNRS, Université de Toulouse, IMRCP-UMR 5623, F31062 Toulouse, France

[c] School of Chemistry and Biochemistry, Georgia Institute of Technology, 901 Atlantic Drive, Atlanta, Georgia 30332-0400, United States

[d] Summer program participant (high school student) from Phillips Exeter Academy, 20 Main St, Exeter, New Hampshire 03833, United States

[e] Physical and Materials Chemistry Division, CSIR-National Chemical Laboratory, Pune 411008, India.

[f] Service commun RX, Institut de Chimie de Toulouse, ICT- FR2599, Université Paul Sabatier 31062 Toulouse cedex 9, France.

[g] CNRS, SPCMIB-UMR 5068, F31062 Toulouse, France

[h] Université Paul Sabatier, SPCMIB-UMR 5068, F31062 Toulouse, France

[i] Olis Inc., 130 Conway Dr, Bogart, Georgia 30622, United States

[#] Contributed equally

ABSTRACT

Four benzoxazole-substituted GFP chromophores that differ by the length of their alkyl chain (from C1 to C12) were synthesized. In solution, the four compounds showed identical spectroscopic behavior, emitting blue light with moderate quantum yield. In the solid state, the butyl, pentyl and dodecyl derivatives strongly emitted orange light, while the methyl derivative was only weakly emissive. Based on the X-ray data and DFT calculations, emission in the solid state was explained by the formation of excimers. A very unusual "hot-dog"-type excimer was found for the dodecyl derivative, in which two overlapping chromophores are separated by an alkyl chain.

INTRODUCTION

The recent discovery of compounds that exhibit aggregation-induced emission (AIE) has opened new avenues in the challenging field of fluorescent materials.[1] Considering the number of potential applications, new varieties are in high demand. A popular strategy consists of bringing modifications to basic chemical structures that have been reported to show AIE behavior in order to optimize the spectroscopic properties.

The green fluorescent protein (GFP) is widely used in biology as a fluorescent marker.[2] Some synthetic derivatives of the GFP chromophore, *p*-hydroxybenzylideneimidazolinone (HBDI), are known to be highly fluorescent when constrained, either covalently within the native *β*-barrel,[3] or by complexation in a protein host.[4] A very recent review from some of us

summarized the utilization of synthetic GFP chromophores for fluorescence imaging.[5] It has also been shown that GFP chromophore derivatives exhibit the AIE effect in the solid state,[6] and all recent examples of AIE-active GFP chromophores were reported in this review. The AIE behavior is dependent on, and can be controlled by, the reprecipitation conditions.[7] In most cases, the GFP chromophores have a moderate photoluminescence quantum yield[7] and emission is often restricted to the blue-green part of the visible spectrum, although a few derivatives show red emission due to the formation of excimers.[5] In a continuing effort to understand the behavior of AIE-active GFP chromophores and to expand this class of compounds, we have synthesized a new set of GFP chromophore derivatives which incorporate a benzoxazole group on the phenyl ring (Fig. 1).

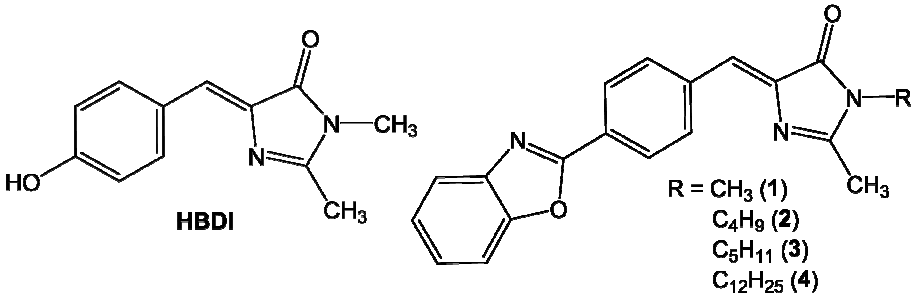

Fig. 1 Structures of *p*-hydroxybenzylideneimidazolinone (HBDI) and benzoxazole-containing GFP chromophores (**1**-**4**).

The aim was to improve the spectroscopic properties of the GFP chromophores by incorporating the 2-phenylbenzoxazole fragment widely employed as a key structure in many fields, i.e. pH and metal cation indicators,[8,9] electrooptics materials,[10] excited-state intramolecular proton transfer (ESIPT) dyes, and metal chelates[11, 12] that can be used for

bioimaging applications. Dyes based on 2-phenylbenzoxazole are generally very stable. They often exhibit excellent fluorescence efficiency in solution and/or in the solid state,[13-15] and AIE behavior has already been reported for a few of them.[9, 16-19] The introduction of the benzoxazole group into the molecular structure of the GFP chromophore was expected to redshift the emission through efficient extension of electron conjugation, and possibly increase the emission quantum yield. The effect on the AIE behavior was unpredictable.

These isoelectronic chromophores all share the same general structure, with each derivative containing a different alkyl chain at the R^1 position (methyl, *n*-butyl, *n*-pentyl and *n*-dodecyl for compounds **1**, **2**, **3**, and **4**, respectively). These small chemical modifications were introduced since they are known to strongly affect the molecular packing mode and hence the solid-state emission properties.

We show that these derivatives not only "turn on" fluorescence in the solid state, exhibiting significant changes in excitation and emission properties compared to that in solution, but they also display strong emission in the orange-red region. In addition, they exhibit formation of a unique excimer, despite an unconventional stacking motif of the crystal structure. To our knowledge, such changes in spectral properties and crystal structure packing have not been reported for GFP-like chromophores.

EXPERIMENTAL SECTION

Synthesis, procedures, and characterization

Chemicals. All the raw materials and analytical grade solvents were used without further purification. 2-Aminophenol (99%), *p*-toluoyl chloride (99%), acetic anhydride (99.5%), sulfuric acid (99%), pyridine (99%), chromium trioxide (98%), glycine methylester hydrochloride (99%), ethylacetimidate hydrochloride (97%), potassium carbonate (99%), N-methylpyrrolidinone, absolute ethanol, and dichloromethane were purchased from Sigma Aldrich. Ethylacetate was obtained from Fisher Scientific. *n*-Methylamine (40% in methanol, ca. 9.8 mol/L), *n*-butylamine (99%), *n*-pentylamine (98%) and *n*-dodecylamine (97%) were purchased from TCI Europe.

Apparatus. The melting points were measured on a Stuart Automatic SMP40 apparatus. Chemical characterizations were performed in the relevant "Service Commun de l'Université de Toulouse 3 - Paul Sabatier". The microanalyses were obtained with a CE elemental analyzer EA1112. The ^{1}H and ^{13}C NMR spectra were recorded on a Bruker AC300 spectrometer operating at 300.13 and 75.48 MHz, respectively. Proton and carbon numbering is indicated in Fig. S1 (Electronic Supplementary Information, ESI). Attributions of ^{13}C signals were made using 2D NMR data (HMBC and HSQC). High resolution mass spectra were recorded with a Waters GCT Premier spectrometer using the chemical ionization technique with CH_4.

Preparation of 2-(4'-formylphenyl)benzoxazole. 2-(4'-Tolyl)-benzoxazole was obtained by stoichiometric condensation of 2-aminophenol with *p*-toluoyl chloride, according to a previously reported procedure.[13] An oxidation was performed in the presence of CrO_3/acetic anhydride to give 2-(4'-formylphenyl)benzoxazole.[20] The characteristics of the obtained compound were identical to those given in the literature.[19, 21]

General procedure for synthesis of the imino derivatives of 2-phenylbenzoxazole.

An aliquot of 2-(4'-formylphenyl)benzoxazole (0.18 g, 0.78 mmol) and a stoichiometric amount of alkylamine were placed in a vial, and solubilized with 10 mL methanol. Depending on the alkylamine used, addition of several drops of dichloromethane was necessary to obtain a clear solution. The yellow solution was stirred at room temperature for 15 h. The solvent was evaporated, and the obtained yellow solid was dried under vacuum at 45°C. The yield was between 90 and 95%. The ^{1}H NMR data for N-[4-(1,3-benzoxazol-2-yl)phenyl]methylidene-alkylamines was reported in the ESI section.

General procedure for synthesis of compounds 1 to 4. Methyl[(1-ethoxyethylidene)amino]acetate was prepared as previously described.[22] It was dissolved in methanol to produce a solution at 0.70 mol/L. A small volume of this solution (1.26 mL, 0.86 mmol) was mixed with 0.78 mmol of N-[4-(1,3-benzoxazol-2-yl)phenyl]methylidene-alkylamine. The obtained suspension was dissolved in 10 mL methanol, with a few drops of dichloromethane to obtain a clear solution if necessary. The yellow solution was stirred at room temperature for 18 h. The solvent was removed under vacuum; the colored solid was triturated with 5 mL diethyl ether and isolated by filtration. It was recrystallized in methanol/THF (70:30 v/v) mixture and dried under vacuum. The yield was between 75 and 83 %.

5-[4-(1,3-Benzoxazol-2-yl)benzylidene]-2,3-dimethyl-3,5-dihydro-4*H*-imidazol-4-one (1)

Mp = ~170 °C (dec). Elemental analysis (%): calculated for $C_{19}H_{15}N_3O_2$: C, 71.91; H, 4.76; N, 13.24; found: C, 71.33; H, 4.44; N, 12.82. ^{1}H NMR (300 MHz, $CDCl_3$) δ (ppm) 8.30 (m, 4H,

$H_{2'}$, $H_{3'}$, $H_{5'}$ and $H_{6'}$), 7.83-7.79 (m, 1H, H_7), 7.63-7.60 (m, 1H, H_4), 7.40-7.37 (m, 2H, H_5 and H_6), 7.13 (s, 1H, $H_{7'}$), 3.22 (s, 3H, N-CH_3), 2.43 (s, 3H, CH_3). ^{13}C NMR (75 MHz, $CDCl_3$) δ (ppm) 170.57 (Cq, $C_{2''}$), 163.76 (Cq, $C_{4''}$), 162.52 (Cq, C_2), 150.84 (Cq, C_8), 142.20 (Cq, C_9), 139.95 (Cq, $C_{1''}$), 137.19 (Cq, $C_{4'}$), 132.44 (CH, $C_{3'}$ and $C_{5'}$), 127.84 (Cq, $C_{1'}$), 127.75 (CH, $C_{2'}$ and $C_{6'}$), 125.58 (CH, $C_{7'}$), 125.43 (CH, C_6), 124.74 (CH, C_5), 120.16 (CH, C_7), 110.69 (CH, C_4), 26.68 (N-CH_3), 15.80 (CH_3). HRMS (DCI-CH_4): *m/z*: calcd for $C_{19}H_{16}N_3O_2$: 318.1243; found: 318.1244 ($M + H^+$).

5-[4-(1,3-Benzoxazol-2-yl)benzylidene]-3-butyl-2-methyl-3,5-dihydro-4*H*-imidazol-4-one (2)

Mp = 147.1 °C. Elemental analysis (%): calculated for $C_{22}H_{21}N_3O_2$: C, 73.52; H, 5.89; N, 11.69; found: C, 73.10; H, 5.83; N, 11.57. ^{1}H NMR (300 MHz, $CDCl_3$) δ (ppm) 8.31 (m, 4H, $H_{2'}$, $H_{3'}$, $H_{5'}$ and $H_{6'}$), 7.84-7.80 (m, 1H, H_7), 7.64-7.61 (m, 1H, H_4), 7.43-7.38 (m, 2H, H_5 and H_6), 7.13 (s, 1H, $H_{7'}$), 3.64 (t, ^3J = 7.3 Hz, 2H, N-CH_2), 2.46 (s, 3H, CH_3), 1.64 (m, 2H, N-CH_2-$C\underline{H}_2$), 1.42 (m, 2H, $C\underline{H}_2$-CH_3), 1.00 (t, ^3J = 7.4 Hz, 3H, CH_2-$C\underline{H}_3$). ^{13}C NMR (75 MHz, $CDCl_3$) δ (ppm) 170.63 (Cq, $C_{2''}$), 163.81 (Cq, $C_{4''}$), 162.55 (Cq, C_2), 150.85 (Cq, C_8), 142.22 (Cq, C_9), 139.92 (Cq, $C_{1''}$), 137.28 (Cq, $C_{4'}$), 132.41 (CH, $C_{3'}$ and $C_{5'}$), 127.82 (Cq, $C_{1'}$), 127.77 (CH, $C_{2'}$ and $C_{6'}$), 125.43 (CH, $C_{7'}$), 125.39 (CH, C_6), 124.74 (CH, C_5), 120.17 (CH, C_7), 110.69 (CH, C_4), 40.53 (N-CH_2), 31.44 (N-CH_2-$\underline{C}H_2$), 20.03 ($\underline{C}H_2$-CH_3), 15.90 (CH_3), 13.70 (CH_2-$\underline{C}H_3$). HRMS (DCI-CH_4): *m/z*: calcd for $C_{22}H_{22}N_3O_2$: 360.1712; found: 360.1720 ($M + H^+$).

5-[4-(1,3-Benzoxazol-2-yl)benzylidene]-3-pentyl-2-methyl-3,5-dihydro-4*H*-imidazol-4-one (3)

Mp = 145.1 °C. Elemental analysis (%): calculated for $C_{23}H_{23}N_3O_2$: C, 73.97; H, 6.21; N, 11.25; found: C, 73.72; H, 6.25; N, 11.31. ^{1}H NMR (300 MHz, $CDCl_3$) δ (ppm) 8.31 (m, 4H, $H_{2'}$, $H_{3'}$, $H_{5'}$ and $H_{6'}$), 7.84-7.81 (m, 1H, H_7), 7.64-7.61 (m, 1H, H_4), 7.43-7.38 (m, 2H, H_5 and H_6), 7.13 (s, 1H, $H_{7'}$), 3.63 (t, ^3J = 7.2 Hz, 2H, N-CH_2), 2.46 (s, 3H, CH_3), 1.67 (m, 2H, N-CH_2-$C\underline{H}_2$), 1.36 (m, 4H, $C\underline{H}_2$-$C\underline{H}_2$-CH_3), 0.94 (t, ^3J = 7.2 Hz, 2H, CH_2-$C\underline{H}_3$). ^{13}C NMR (75 MHz, $CDCl_3$) δ (ppm) 170.63 (Cq, $C_{2''}$), 163.85 (Cq, $C_{4''}$), 162.55 (Cq, C_2), 150.84 (Cq, C_8), 142.21 (Cq, C_9), 139.91 (Cq, $C_{1''}$), 137.28 (Cq, $C_{4'}$), 132.42 (CH, $C_{3'}$ and $C_{5'}$), 127.81 (Cq, $C_{1'}$), 127.78 (CH, $C_{2'}$ and $C_{6'}$), 125.46 (CH, $C_{7'}$), 125.42 (CH, C_6), 124.76 (CH, C_5), 120.17 (CH, C_7), 110.71 (CH, C_4), 40.76 (N-CH_2), 29.08 (N-CH_2-$C\underline{H}_2$), 28.89 ($C\underline{H}_2$-CH_2-CH_3), 22.34 ($C\underline{H}_2$-CH_3), 15.93 (CH_3), 13.98 (CH_2-$C\underline{H}_3$). HRMS (DCI-CH_4): *m/z*: calcd for $C_{23}H_{24}N_3O_2$: 374.1869; found: 374.1877 ($M + H^+$).

5-[4-(1,3-Benzoxazol-2-yl)benzylidene]-3-dodecyl-2-methyl-3,5-dihydro-4*H*-imidazol-4-one (4)

Mp = 113.4 °C. Elemental analysis (%): calculated for $C_{30}H_{37}N_3O_2$: C, 76.40; H, 7.91; N, 8.91; found: C, 76.06; H, 7.84; N, 8.89. ^{1}H NMR (300 MHz, $CDCl_3$) δ (ppm) 8.35 (m, 4H, $H_{2'}$, $H_{3'}$, $H_{5'}$ and $H_{6'}$), 7.84-7.81 (m, 1H, H_7), 7.65-7.62 (m, 1H, H_4), 7.42-7.39 (m, 2H, H_5 and H_6), 7.13 (s, 1H, $H_{7'}$), 3.67 (t, ^3J = 7.3 Hz, 2H, N-CH_2), 2.45 (s, 3H, CH_3), 1.67 (m, 2H, N-CH_2-$C\underline{H}_2$), 1.34 (m, 18H, CH_2), 0.91 (t, ^3J = 7.3 Hz, 3H, CH_3). ^{13}C NMR (75 MHz, $CDCl_3$) δ (ppm) 170.62 (Cq, $C_{2''}$), 163.85 (Cq, $C_{4''}$), 162.56 (Cq, C_2), 150.85 (Cq, C_8), 142.21 (Cq, C_9), 139.92 (Cq, $C_{1''}$), 137.28 (Cq, $C_{4'}$), 132.42 (CH, $C_{3'}$ and $C_{5'}$), 127.84 (Cq, $C_{1'}$), 127.78 (CH, $C_{2'}$ and $C_{6'}$), 125.44 (CH, $C_{7'}$), 125.41 (CH, C_6), 124.76 (CH, C_5), 120.17 (CH, C_7), 110.70 (CH, C_4), 40.81 (N-CH_2), 31.94 (N-CH_2-$C\underline{H}_2$), 30.90 (CH_2), 29.64 (CH_2), 29.58 (CH_2), 29.51 (CH_2), 29.40 (CH_2), 29.37

(CH_2), 29.26 (CH_2), 26.81 ($\underline{C}H_2$-CH_2-CH_3), 22.72 ($\underline{C}H_2$-CH_3), 15.94 (CH_3), 14.17 (CH_2-$\underline{C}H_3$). HRMS (DCI-CH_4): *m/z*: calcd for $C_{30}H_{38}N_3O_2$: 472.2964; found: 472.2985 ($M + H^+$).

Crystallographic data

Single crystals of compounds **1** and **3** were grown in methanol; crystals of **2** and **4** were grown in tetrahydrofuran and ethanol, respectively. Crystal data were collected at a temperature of 193 K on a Bruker-AXS kappa APEX II Quazar diffractometer using a 30 W air-cooled microfocus source (ImS) with focusing multilayer optics using MoKα radiation (wavelength = 0.71073 Å). Phi- and omega-scans were used. The structures were solved by direct methods and all non-hydrogen atoms were refined anisotropically using the least-square method on F^2.[23] Molecular views and crystal data of compounds **1**-**4** are given in Fig. S2 and Table S1 (ESI).

These data can be obtained free of charge via www.ccdc.cam.ac.uk/data_request/cif (or for the CCDC, 12 Union Road, Cambridge CB21EZ, UK; fax: +441223 336033; e-mail: deposit@ccdc.cam.ac.uk).

Spectroscopy

Spectroscopic measurements were conducted at 20°C in a temperature-controlled cell. Ultraviolet-visible spectra were recorded on a Perkin Elmer Lambda19 spectrophotometer. Fluorescence work in solution was performed with a Xenius SAFAS spectrofluorometer using cells of 1 cm optical pathway. All fluorescence spectra were corrected. The fluorescence quantum yields (Φ_F) were determined using the classical formula: $\Phi_{Fx} = (A_s \times F_x \times n_x^2 \times \Phi_{Fs})/(A_x$

$\times F_s \times n_s^2$) where A is the absorbance at the excitation wavelength, F the area under the fluorescence curve and n the refraction index. Subscripts s and x refer to the standard and to the sample of unknown quantum yield, respectively. Coumarin 102 in ethanol ($\Phi_F = 0.764$) was used as the standard.[24] The fluorescence quantum yields were measured by exciting the samples at 384 nm. The absorbance of the solutions was equal or below 0.055 at the excitation wavelength. The error on the quantum yield values is estimated to be about 10 %. The measurement of the photoluminescence quantum yields on powder compounds was performed with the same apparatus. Solid samples were deposited on a metal support and introduced in a $BaSO_4$ integrating sphere. The excitation source was scanned in order to evaluate the reflected light for the empty sphere (L_a), the samples facing the source light (L_c) and the sample out of the irradiation beam (L_b). The fluorescence spectra were recorded with the sample facing the source light (E_c) and out from the direct irradiation (E_b). The PM voltage was adapted to the measurement of reflected light and emission spectra, respectively, and proper correction was applied to take into account the voltage difference. The absolute photoluminescence quantum yield values (Φ_P) were determined by a method based on the one developed by de Mello *et al.*,[25] using the formula:

$$\Phi_P = [E_c - (1 - \alpha)\, E_b] / L_a\, \alpha$$

with $\alpha = 1 - L_c / L_b$

Solution spectra and measurements of solid-state photoluminescence were also carried out using a Jobin-Yvon FluoroLog-3 spectrofluorimeter, especially for excitation-emission matrix spectroscopy. For photoluminescence, the front face emission scan mode was used. The entrance/exit slits of the monochromators were adjusted to the proper fluorescence intensity of each sample. Crystalline powder samples were placed between quartz plates. Fluorescence

lifetimes were measured using an Edinburgh Instruments time-correlated single photon counting (TCSPC) system. In this measurement, two picosecond excitation pulse diode lasers (LDH-P-C-375 and LDH-P-C-470) with different wavelengths (372 nm and 467 nm) were used as excitation light sources. The detection system consisted of a high speed MicroChannel Plate PhotoMultiplier Tube (MCP-PMT, Hamamatsu R3809U-50) and TCSPC electronics.

Computational methods

We performed calculations at B3LYP/6-311++G(d,p) and CAM-B3LYP/6-311++G(d,p) levels of theory on HBDI chromophores as well as Chr 1-4 monomers to calculate their absorption and emission peak positions in gas phase. The CAM-B3LYP and B3LYP calculations were in good agreement with the previous theoretical results on gas phase HBDI and experimental results.[26] To estimate the effect of solvation on the absorption and emission peaks, the B3LYP/6-31+G(d,p) level of theory with SM8 solvation model was used. The estimates for solid state structures were computed for dimer/trimer calculations from crystal structure.

RESULTS AND DISCUSSION

Synthesis

Chromophores for this work (**1-4**) were synthesized as follows (ESI, Fig. S3,): 2-(4'-Formylphenyl)benzoxazole was condensed with a primary alkylamine (methylamine, *n*-butylamine, *n*-pentylamine, *n*-dodecylamine) to give the corresponding imino derivative. These compounds were allowed to react with methyl[(1-ethoxyethylidene)amino]acetate using the [2+3] cycloaddition reaction first reported in 1995 by Bazureau et al.[27] and expanded in 2010 by

the Tolbert lab[21] to form the imidazolinone ring. The compounds were bright yellow powders. They were characterized by ^{1}H NMR and ^{13}C NMR spectrometry. HRMS and microanalysis data for each synthesized derivative indicated a high level of purity.

Spectroscopy

The spectroscopic characteristics of chromophores **1-4** in solution were almost identical. In ethanol, the four compounds exhibited an unstructured absorption band with maxima around 384 nm (ESI, Fig. S4). These spectra were therefore red-shifted by ~90 nm with respect to those of 2-phenylbenzoxazole, and close to those recorded for GFP chromophores.[7,28] The compounds displayed a high magnitude of molar extinction coefficients (~38500 $M^{-1}cm^{-1}$), supporting a strong electron delocalization of their systems. A solvatochromic effect was investigated using compound **2**. It appeared that the shape of the absorption spectrum was almost unchanged in other organic solvents, but the maximum was slightly shifted to a longer wavelength with increasing solvent polarity (Table 1).

Solvent	λ_{abs} (nm)	λ_{ex} (nm)	λ_{em} (nm)	Φ_F
n-heptane	382	380	438	0.028
Ethyl acetate	385	380	446	0.070
Dimethylsulfoxide	390	382	458	0.068
Ethanol	384	384	448	0.017

Table 1 Spectroscopic characteristics of compound **2** dissolved in various organic solvents. Maximum absorption wavelength (λ_{abs}), maximum excitation wavelength (λ_{ex}), maximum

emission wavelength (λ_{em}) and fluorescence quantum yields (Φ_F). For emission spectra, excitation was at 384 nm. For excitation spectra, emission was at 448 nm. Dye concentration around 1.3×10^{-5} M for absorption and 1.3×10^{-6} M for emission measurements.

The four compounds emitted blue fluorescence in solution. In ethanol, the excitation spectra of the four compounds were very close to the absorption spectra, and the emission spectra showed a single band with an emission maximum at 448 nm (ESI, Fig. S5). The fluorescence quantum yields were found to be 0.020, 0.017, 0.021 and 0.019 for compounds **1**, **2**, **3** and **4**, respectively, meaning that they were almost identical considering the measurement error.

The nature of the solvent had moderate effect on the fluorescence spectra, as exemplified with **2** in Fig. 2. All the excitation spectra were very close as well. A small shift was noticed between excitation and absorption spectra in dimethylsulfoxide (Table 1), suggesting the involvement of various conformations in this medium. The emission spectra were shifted by 20 nm to the red with increasing polarity. The quantum yields were quite low in a non-polar solvent like *n*-heptane, but they were increased in solvents of moderate and strong polarity such as ethylacetate and dimethylsulfoxide, and were decreased again in a protic solvent like ethanol. The quantum yields were in the 10^{-2} range, so they were lower by one order of magnitude than that of 2-phenylbenzoxazole,[13] but much higher than those of GFP chromophore derivatives in solution, which are in the 10^{-4} range.[7, 29, 30] Simple 2-phenylbenzoxazole derivatives are usually hardly affected by the medium proticity,[13] so the loss of fluorescence efficiency observed here in ethanol can be attributed to the formation of hydrogen bonds between the solvent and the GFP moiety. This implies that in solution the behavior of compounds **1**-**4** is intermediate between that

of both moieties that constitute the molecules. It is interesting that the spectral shape of the absorption and the emission spectra, as well as the corresponding spectral maxima were very close to those of para-substituted BDI chromophores. This indicates a surprisingly weak degree of conjugation between the BDI and phenylbenzoxazole moieties in solution.

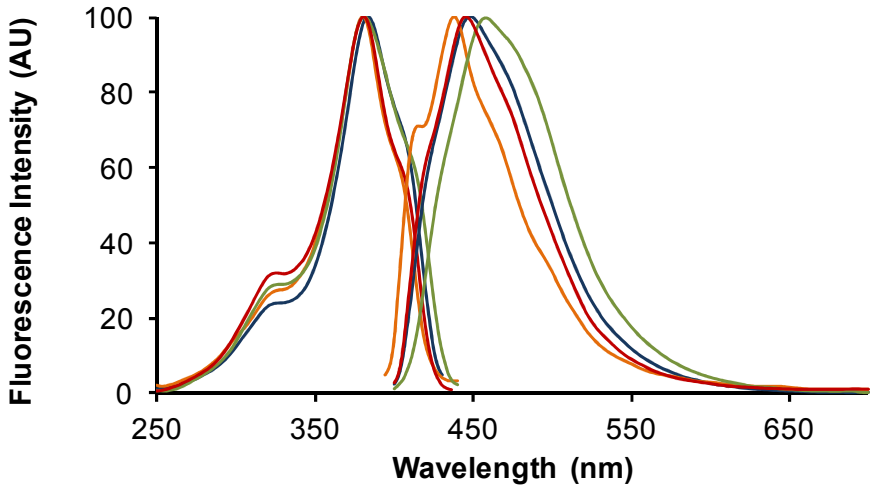

Fig. 2 Normalized excitation (λ_{em} = 446 nm) and emission (λ_{ex} = 384 nm) spectra of compound **2** in *n*-heptane (orange line), ethylacetate (red line), ethanol (blue line), and dimethylsulfoxide (green line). Dye concentration around 1.5 $\times 10^{-6}$ M.

Solid-state spectroscopic studies were performed on the microcrystalline powders that had been obtained by organic solvent evaporation at the end of the recrystallization process. It must be emphasized that, most probably, different values would have been found with single crystals as well as with powders prepared from recrystallization in other solvents, sublimation or by mechanical milling, since impurities and surface defect play an essential role in solid-state emission properties.[31]

The powders of compounds **2**-**4** exhibited strong yellow to orange light emission under a hand-held UV lamp. In contrast, the short chain derivative **1** was only weakly photoluminescent. The solid-state emission properties were first studied with a fluorimeter equipped with an integrating sphere. The emission spectra of compounds **2**-**4**, recorded by exciting at 384 nm, were similar. They showed a dual emission with a narrow, intense band centered around 612 nm, and a very weak band at a shorter wavelength, around 490 nm (Fig. 3). The long-chain derivatives thus showed a clear shift in emission towards long wavelengths, when comparing the solid state spectrum to the solution spectrum. Under the same experimental conditions, the emission spectra of **1** showed two very weak bands at 612 and between 450 and 490 nm. The difference between the solution and solid state spectroscopic properties was therefore much stronger for the long chain analogs than for the methyl derivative. The photoluminescence quantum yields quantified the difference of behavior between the compounds. They were 0.16, 0.18 and 0.26 for **2**, **3** and **4**, respectively, and below 10^{-3} for **1**. The solid-state spectroscopic data are summarized in Table S2(ESI).

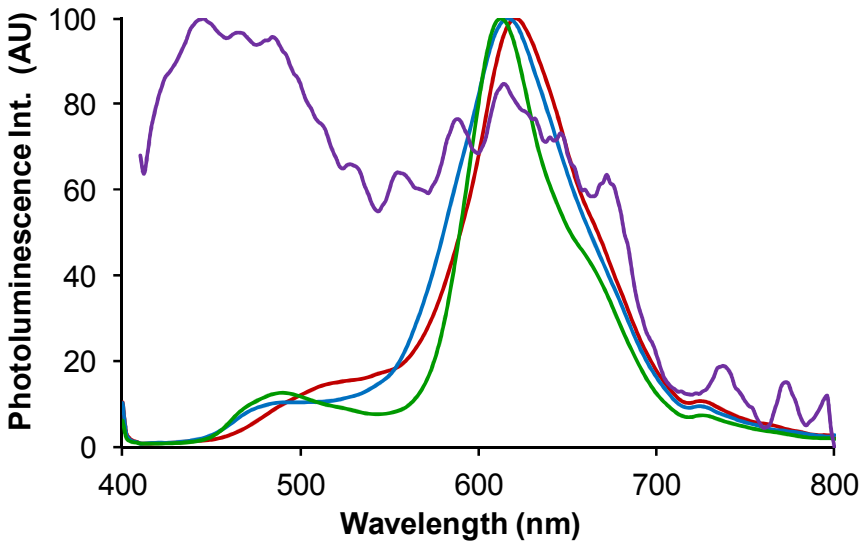

Fig. 3 Normalized photoluminescence spectra (λ_{ex} = 384 nm) of powder compounds **1** (purple line), **2** (red line), **3** (blue line), and **4** (green line).

To reveal the possible complex nature of multispecies solid-state emission, we collected fluorescence excitation-emission matrix spectra (Fig. 4). For compounds **2-4** the contour plots were very similar, confirming two emitting centers with dominating emission in the orange. Importantly, both long- and short-wavelength peaks exhibited the same excitation spectra, which were very close to those observed in solutions but slightly red shifted (ESI, Fig. S7 to S9). The very weak solid-state emission behavior of **1** is more complex than that of compounds **2-4** since it includes a 470/600 ex/em spectral feature, which demonstrates a presence of totally different ground-state absorbing species in the powder of **1** (ESI, Fig. S6).

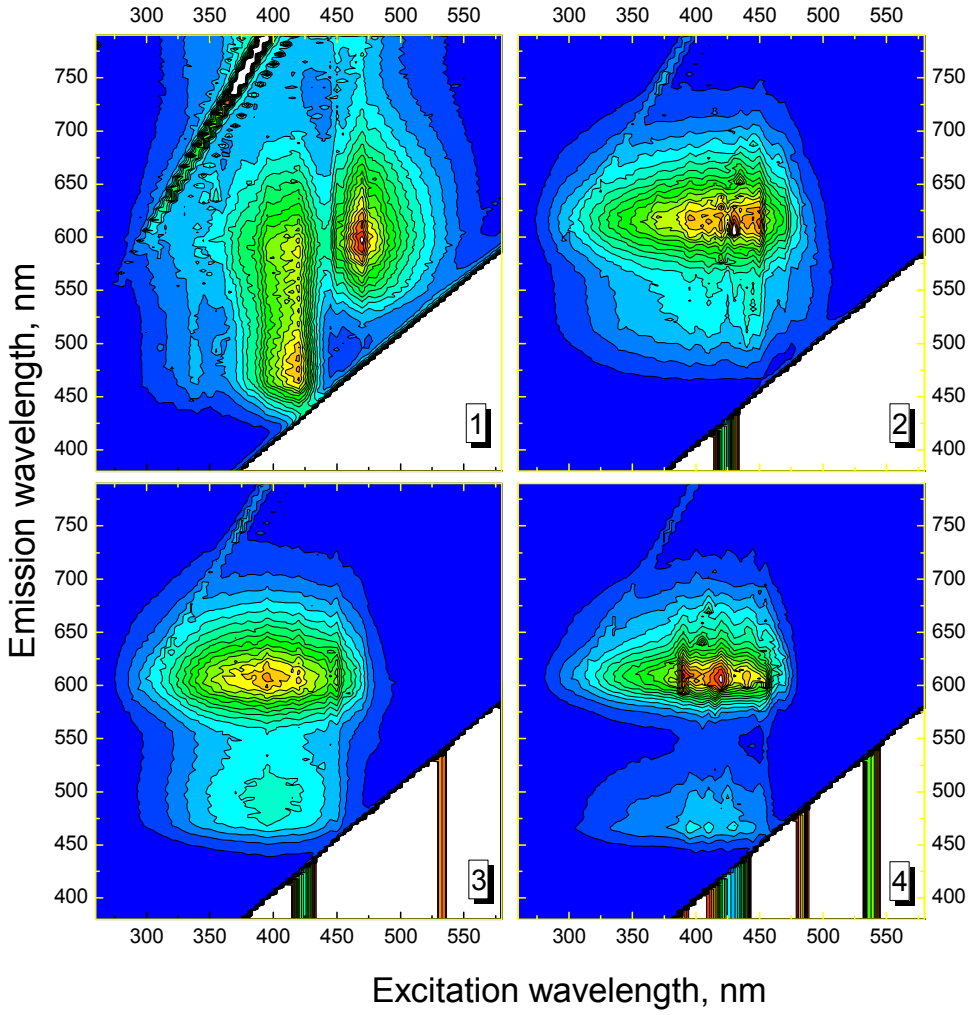

Fig. 4 Excitation-emission matrix spectra of the four compounds in the solid state.

The fluorescence kinetic measurements in the solid state indicated that the lifetimes of the red-shifted species were far longer than those of the shorter-wavelength emitting species. The trend of longer lifetime for the red-shifted emission was conserved throughout the series of compounds. However, with shorter alkyl chains, the lifetimes also became shorter, as can be seen by contrasting the decay profiles of the *N*-dodecyl chromophore with that of the *N*-methyl chromophore (Fig. 5). For the kinetic spectra of all compounds, see the ESI section.

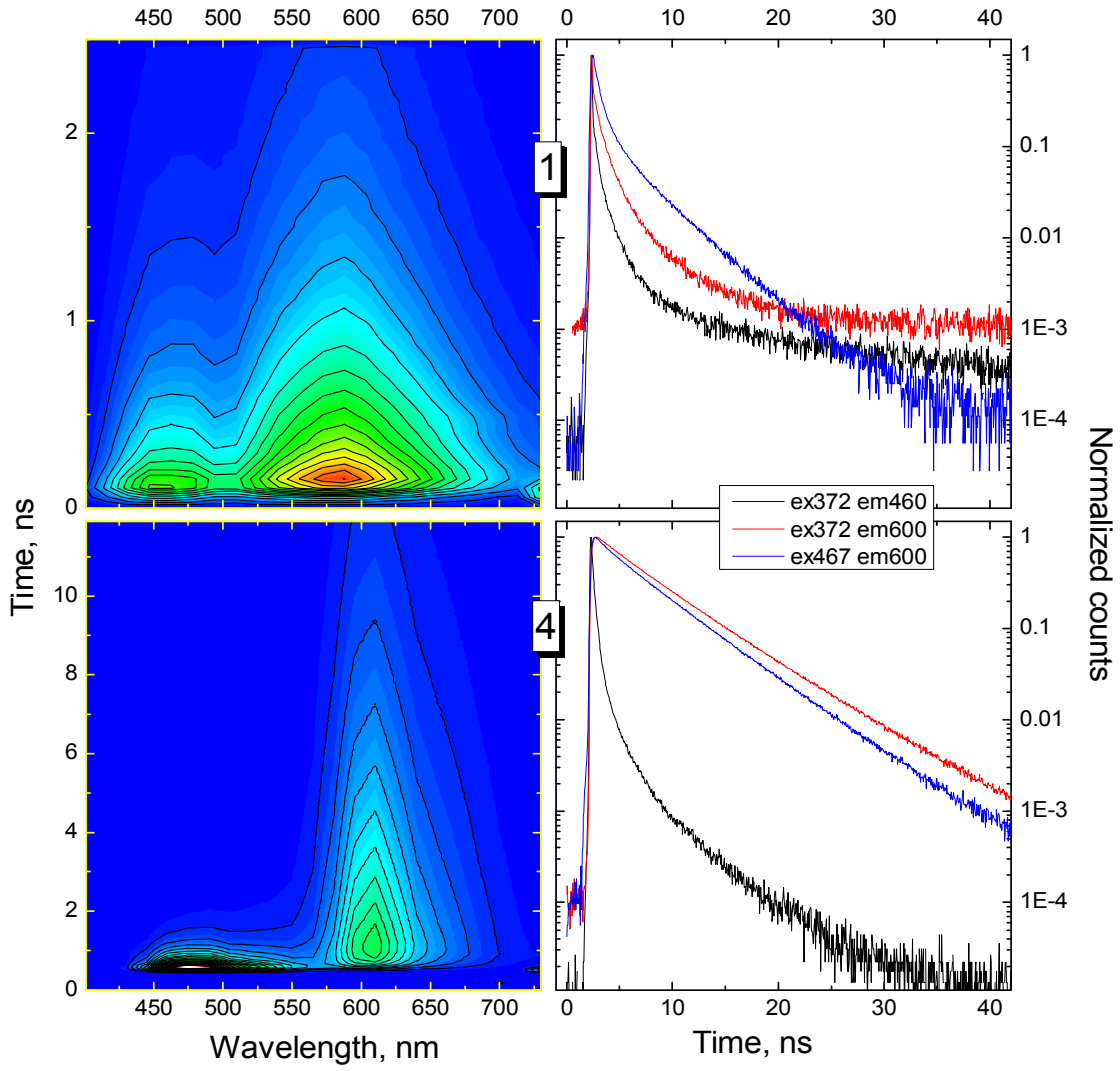

Fig. 5 Left: Fluorescence decay surfaces of compounds **1** and **4** in the microcrystalline powder state, taken with 372 nm laser excitation. Right: Selected kinetic traces.

At this stage, it can be hypothesized that this long-lived, red-shifted emission must be caused by an excimer formed in the solid state, due to the aggregation of the molecules. In contrast, the short-lived, short-wavelength emission apparently arises from molecules that

behave like dissolved molecules, whether they belong to crystal defects or just behave as monomers.

The clear and distinct appearance of well-separated emission centers in the solid-state emission of the BDI derivatives is unique, since in two known cases of spectral broadening no distinct new bands were detected.[6,32] Also of note is that this phenomenon cannot be caused simply by the presence of long alkyl chains on the imidazolidinone ring, because as reported by Shen, *et al.*,[33] introduction of long alkyl chains at the C-terminus does not result in drastic changes in absorbance or emission, although an increase of fluorescent lifetime was observed. Therefore, these dramatic changes in spectral properties must be caused by a combination of both the presence of the benzoxazole moiety on the phenyl ring, perhaps in correlation to the alkoxy derivatives reported by the Tolbert group in 2009,[6] and the long alkyl chain, which has been demonstrated to increase the emission intensity.[33] It is also particularly noteworthy that all four of the compounds discussed herein exhibit this excimeric behavior, but with different efficiency according to the size of the alkyl chain.

Crystal structure

To understand the origin of the spectroscopic behavior of novel solid-state emitters, it was necessary to investigate the molecular arrangement in the solid state, and more particularly the stacking of the aromatic rings, which drastically influences the photoluminescence properties. Fortunately, single crystals suitable for X-ray analysis were obtained for the four compounds. The common feature was an almost planar aromatic moiety of each compound. Apart from this, each compound exhibited a unique crystal structure. The methyl chromophore molecules (**1**) were displayed in the crystal unit according to two distinct planes that formed between them at

an angle of 54°. This “crossed dipole” arrangement was reminiscent of that already found for many benzoxazole and naphthoxazole derivatives.[13, 34] However, this arrangement progressively disappeared with increasing the chain length, the long-chained molecules tending to get aligned according to the same axis (ESI, Fig. S10). Let us turn our attention towards the arrangement of stacking molecules. Compound **1** seemed to be organized in head-to-tail dimers, with strong overlap of the benzo ring of one molecule with the imidazolone ring of the other molecule (Fig. 6). Dimers were slipped with respect to each other, so that molecules belonging to two superimposed dimers had very small overlap. The *N*-butyl chromophore (**2**) showed a head-to-head stacking motif with very little overlap of the aromatic moieties, due to horizontal slippage. The *N*-pentyl derivative (**3**), on the other hand, showed a head-to-tail stacking motif, with no overlap of aromatic moieties. Upon closer look, however, by considering three stacked molecules, it can be seen that there is some overlap of the aromatic moieties of the top and bottom molecules. The *N*-dodecyl chromophore (**4**) also showed a head-to-tail stacking motif and no overlap of aromatic moieties between adjacent molecules. However, there was again significant overlap between the top and bottom molecules. This lack of interaction between adjacent molecules, yet good overlap between every other molecule, is what has led us to term this type of stacking as "hot dog stacking."

The overlap between the aromatic systems of stacked molecules could explain the very low photoluminescence quantum yield of compound **1**. In contrast, the reduced overlap observed for compounds **2**-**4** agrees well with the good luminescence efficiency of these compounds. The question is whether the unique aspect of the hot dog stacking is related to a particular photophysical effect. In this precise case, this would mean that the excimer involves electronic

interaction through the intervening alkyl chains, which to our knowledge has never previously been observed.

Compound	Side view	Top view
1	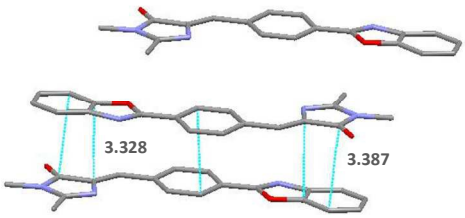	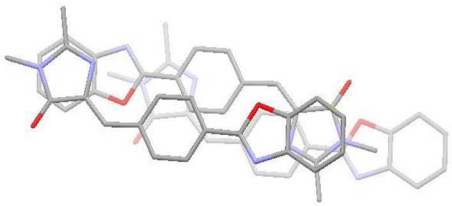
2	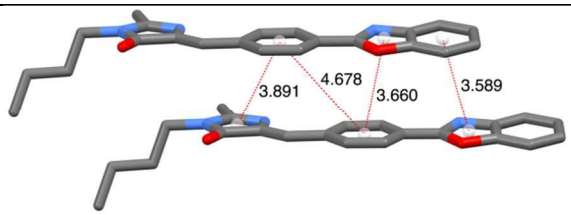	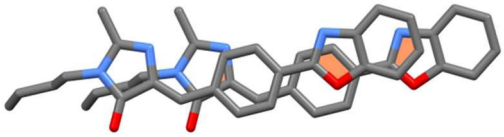
3	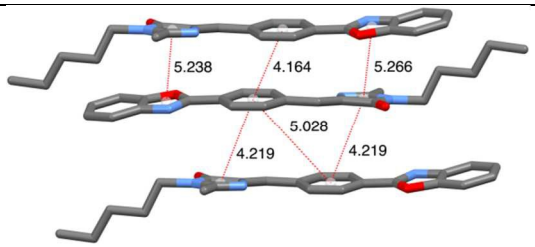	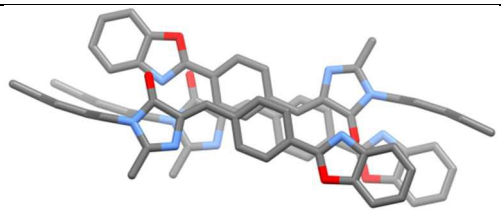
4	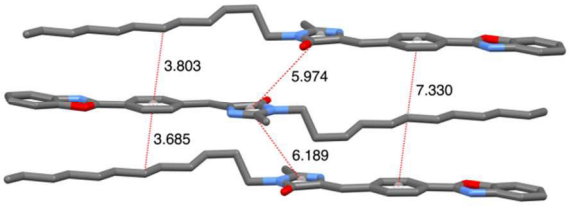	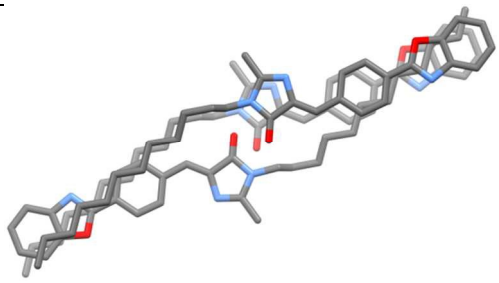

Fig. 6 Side views and top-down views of the crystal structures of compounds **1**-**4**. Distances are shown in angstroms. For **2**, the overlap of aromatic moieties is highlighted in orange. For the other compounds, depth is indicated by color saturation.

Computational results

To evaluate this hypothesis, computations were undertaken. First of all, the levels of theory were benchmarked for neutral HBDI. The vertical excitation energy (VEE) computed with B3LYP/6-311++G(d,p) was found to be 328 nm, in quite good agreement with the experimental observation of 340 nm in vacuum and the earlier theoretical estimate of 324-375 nm.[35]

Calculations were then performed for compounds **1**-**4** in the gas phase and in aqueous solution. For all these compounds, the B3LYP/6-311++G(d,p) absorption peaks (VEE) in the gas phase were within the range of 378-384 nm and the emission maximum was around 413 nm. All these excitations involved HOMO-LUMO type transitions. In solution (SM8 water), the B3LYP/6-31+G(d,p) absorption peak was 373 nm, so very little change was noticed in absorption compared to the gas phase value. However, the emission in water showed two peaks, i.e. a HOMO-(LUMO+1) transition at 532 nm and a (HOMO-1)-LUMO transition at 417 nm, as exemplified for the *N*-methyl compound **1** in Fig. 7.

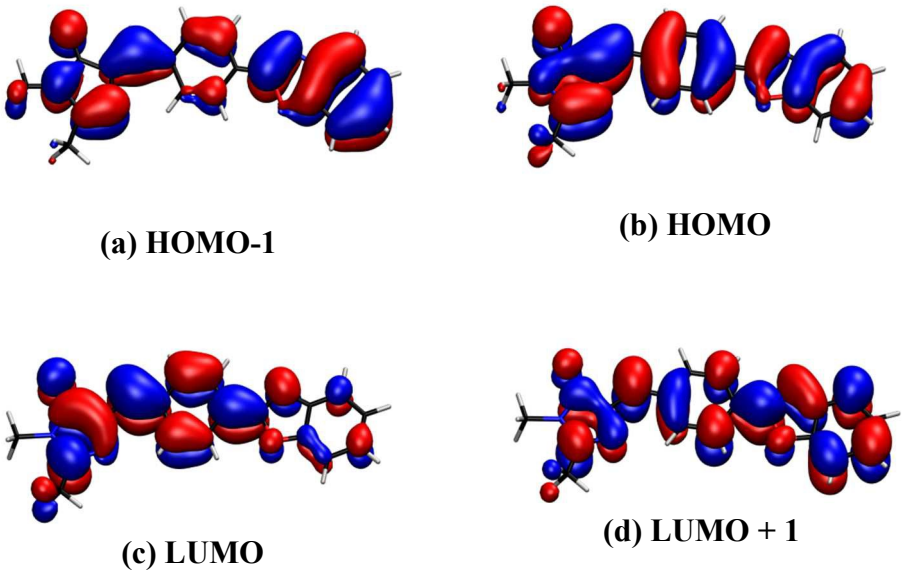

Fig. 7 HOMO-1, HOMO, LUMO and LUMO+1 of compound **1** in solvent (water) calculated at the B3LYP/6-31G* level of theory.

Calculations in the solid state were performed for the *N*-butyl and *N*-dodecyl derivatives, **2** and **4**, respectively, on the basis of X-ray data. The dimer calculation for compound **2** showed HOMO-LUMO absorption at 411 nm while the emission was shifted to 765 nm, which corresponds to an excimer/charge transfer state (Fig. 8). Another emission peak was also observed at 462 nm.

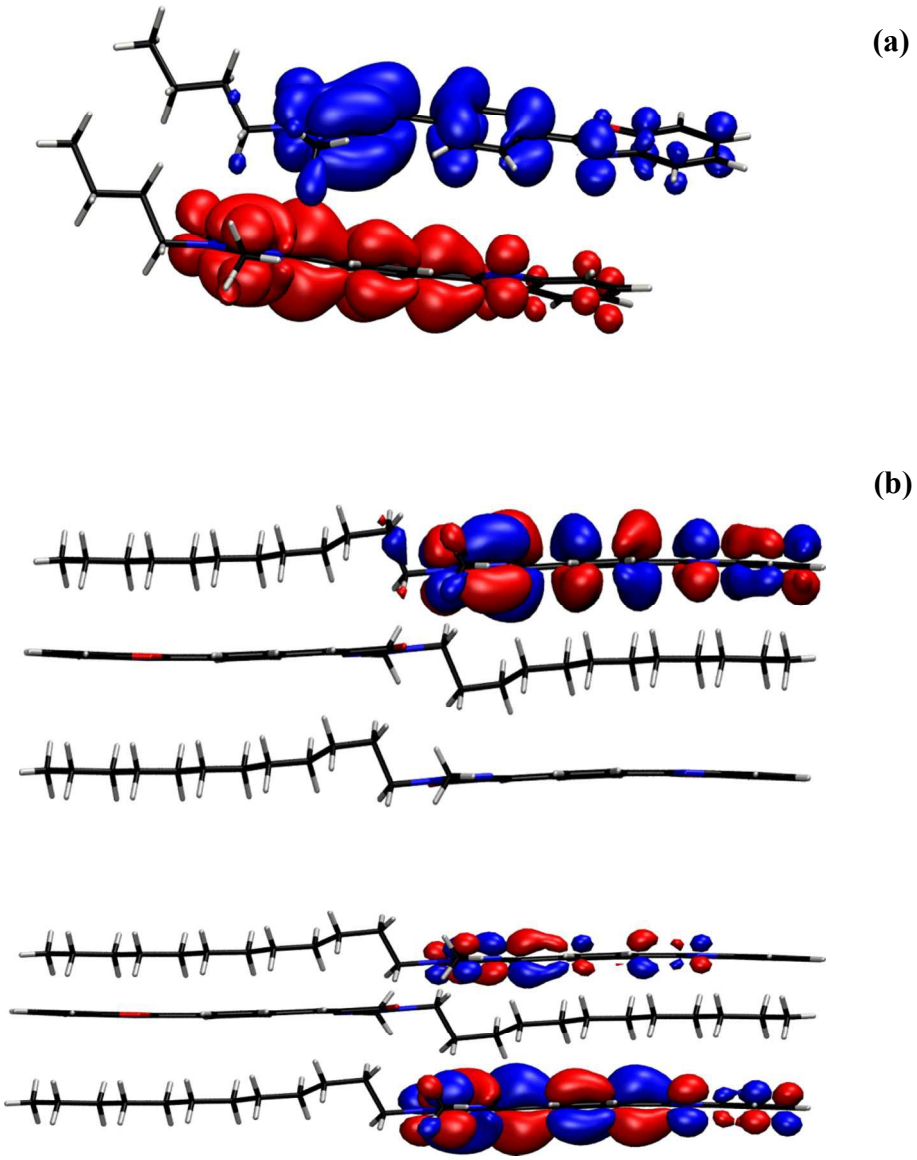

Fig. 8 (a) Attachment-detachment density of the optimized S_1 state of compound **2** shows charge transfer nature. The absorption from S_0 minima is localized. (b) Orbitals from the trimer of compound **4** that are involved in excitation (O1 → O2).

For the large system of compound **4**, the estimated absorption was at 442 nm by considering nearest neighbor and next nearest neighbor interactions, i.e. a trimer. Emission was around 496 nm. Figure 8b shows some charge delocalization in the excited state.

Table 2 summarizes the computational absorption and emission peaks of the chromophores in various media. Absorption did not show any dramatic change on going from gas phase to solution, and then to solid state. The gradual red shift observed in solid state with respect to aqueous solution may be due to more diffuse excitations. This calculated shift is in good agreement with that observed experimentally in the excitation-emission matrix spectra (Fig. 4). Besides, calculated emission showed the appearance of a clear excimer peak at 765 nm for compound **2** in the solid state. This value was quite far from the experimental one (612 nm). The excimer peak of compound **4** in the solid state was less pronounced and situated at shorter wavelengths than the experimental emission peak. This discrepancy is possibly due to the use of a small basis set (absence of diffuse functions) in this trimer calculation.

The calculations also do not explain why the experimental emission peaks of compounds **2**-**4** were quite close while the crystal packing modes were different. Red shifts observed with passing from solution to solid state are generally attributed to *J*-aggregates.[36] In the present case, it would be an over-simplification to say that the molecular arrangement of the three compounds is a mere *J*-aggregate. This shows that the spectroscopic effect results from complex interactions generated by the environment of the fluorophores in a three-dimensional network. The important finding is that, although this type of computation is not very precise at the moment, it indeed indicates the possibility of strong interactions between chromophores even when the aromatic moieties are separated by an alkyl chain.

Compounds	**1-4** (gas phase)	**1-4** (aqueous)	**2** (solid state) Dimer	**4** (solid state) Trimer
Absorption	378-384 nm	~370 nm	411 nm	442 nm
Emission	~413 nm	532, 417 nm	765, 480 nm	496 nm

Table 2 Calculated absorption and emission peaks in various media.

CONCLUSION

A new class of GFP chromophore derivatives based on incorporation of a benzoxazole group was presented. These derivatives do not exhibit pure AIE effect, but rather aggregation enhanced emission, because they are already weakly emissive in solution. They merge the qualities of the C-terminus long-chain chromophores reported by Shen,[33] as they show increased fluorescence intensity in the solid state and longer lifetimes, and those of the phenyl alkoxy chromophores reported by the Tolbert group, as they show significant red-shifting of emission and absorption in the solid state.[6] Above all, their good photoluminescence efficiency is reminiscent of that of 2-phenylbenzoxazole derivatives.[13] In the literature, GFP-like chromophores in which the *p*-hydroxyphenyl group is substituted by a large aromatic moiety do not show any significant increase of fluorescence efficiency in solution, and only the naphthalene derivatives have moderately high quantum yield in the solid state.[32] The 2-phenylbenzoxazole group is therefore of particular interest. Additionally, we observe a new stacking motif, "hot dog stacking", which results in a potential new class of excimers. This study confirms that linking the benzoxazole and GFP chromophore moieties can result in valuable new optical materials.

ACKNOWLEDGEMENTS

We would like to thank Prof. Pance Naumov of New York University at Abu Dhabi and his student Elisa Nauha for their help in interpreting our crystal structure data and extracting bond distances from that data. KMS and LMT acknowledge generous support from the National Science Foundation (CHE-1213047 and CHE-1425951). AG and SFF are very grateful to EuroNanoMed ERA-NET JTC2011 (FONDIAG project) for financial support and to the "Service des Relations Internationales de l'Université de Toulouse III-Paul Sabatier" for the award of travel grants (ATUPS and Amérique du Nord programs).

REFERENCES

(1) Qin, A.; Tang, B. Z. (Eds). *Aggregation-Induced Emission : Fundamentals*, John Wiley & Sons, Ltd., Singapore, **2014**. ISBN 978-1-118-39430-4.

(2) Zimmer, M. *Chem. Rev.* **2002**, *102*, 759-781.

(3) Chen, M. C.; Lambert, C. R.; Urgitis, J. D.; Zimmer, M. *Chem. Phys.* **2001**, *270*, 157-164.

(4) Baldridge, A.; Feng, S.; Chang, Y.-T.; Tolbert, L. M. *ACS Combi. Sci.* **2011**, *13*, 214-217.

(5) Walker, C. L.; Lukyanov, K. A.; Yampolsky, I. V.; Mishin, A. S.; Bommarius, A. S.; Duraj-Thatte, A. M.; Azizi, B.; Tolbert, L. M.; Solntsev, K. M. *Curr. Opin. Chem. Biol*. **2015**, *27*, 64-74.

(6) Dong, J.; Solntsev, K. M.; Tolbert, L. M. *J. Am. Chem. Soc.* **2009**, *131*, 662−670.

(7) Fery-Forgues, S.; Veesler, S.; Fellows, W. B.; Tolbert, L. M.; Solntsev, K. M. *Langmuir* **2013**, *29*, 14718-14727.

(8) Chen, L. N.; Kuo, C. C.; Chiu, Y. C.; Chen, W. C. *RSC Adv.* **2014**, *4*, 45345-45353.

(9) Chen, H.; Feng, Y. ; Deng, G. J.; Liu, Z. X.; He, Y. M., Fan, Q. H. *Chem. Eur. J.* **2015**, *21*, 11018–11028.

(10) Fuks-Janczarek, I.; Kityk, I. V.; Miedziński, R.; Gondek, E.; Ebothe, J.; Nzoghe-Mendome, L.; Danel, A. *J. Mater. Sci.: Mater. Electron.* **2007**, *18*, 519-526.

(11) Wang, J.; Chu, Q.; Liu, X.; Wesdemiotis, C.; Pang, Y. *J. Phys. Chem. B* **2013**, *117*, 4127-4133 and references therein.

(12) Xiao, L.; Sun, S.; Pei, Z.; Pei, Y.; Pang, Y.; Xu, Y. *Biosens. Bioelectron.* **2015**, *65*, 166-170.

(13) Ghodbane, A.; D'Altério, S.; Saffon, N.; McClenaghan, N. D.; Scarpantonio, L.; Jolinat, P.; Fery-Forgues, S. *Langmuir* **2012**, *28*, 855-863 and references therein.

(14) Ghodbane, A.; Saffon, N.; Blanc, S.; Fery-Forgues, S. *Dyes Pigm.* **2015**, *113*, 219-226.

(15) Benelhadj, K.; Muzuzu, W.; Massue, J.; Retailleau, P.; Charaf-Eddin, A.; Laurent, A. D.; Jacquemin, D.; Ulrich, G.; Ziessel, R. *Chem. Eur. J.* **2014**, *20*, 12843-12857.

(16) Wang, L.; Shen, Y.; Yang, M.; Zhang, X.; Xu, W.; Zhu, Q.; Wu, J.; Tian, Y.; Zhou, H. *Chem. Commun.* **2014**, *50*, 8723-8726.

(17) Yadav, U. N., Kumbhar, H. S., Deshpande, S. S. ; Sahoo, S. K. ; Shankarling, G. S. *RSC Adv.* **2015**, *5*, 42971-42977.

(18) Li, G.; Zhu, D.; Liu, Q.; Xue, L.; Jiang, H. *Org. Lett.* **2013**, *15*, 924-927.

(19) Wang, L.; Zheng, Z.; Yu, Z.; Zheng, J.; Fang, M.; Wu, J.; Tian, Y.; Zhou, H. *J. Mater. Chem. C* **2013**, *1*, 6952-6959.

(20) Huber, U. *Patent PCT Int. Appl.* 2004000256. 31-12-2003.

(21) Thomas, D. A. *J. Heterocycl. Chem.* **1970**, *7*, 457-462.

(22) Baldridge, A.; Kowalik, J.; Tolbert, L. M. *Synthesis.* **2010**, *14*, 2424-2436.

(23) Sheldrick, G.M. *Acta Cryst. A* **2008**, *64*,112-122.

(24) Rurack, K.; Spieles, M. *Anal. Chem.* **2011**, *83*, 1232-1242.

(25) De Mello, J. C.; Wittmann, F. H.; Friend, R. H. *Adv. Mater.* **1997**, *9*, 230-232.

(26) Greenwood, J. B.; Miles, J.; De Camillis, S.; Mulholland, P; Zhang, L.; Parkes, M. A.; Hailes, H. C.; Fielding, H. H. *J. Phys. Chem. Lett.*, **2014**, *5*, 3588–3592.

(27) Lerestif, J. M.; Perrocheau, J.; Tonnard, F.; Bazureau, J. P.; Hamelin, J. *Tetrahedron.* **1995**, *24*, 6757-6774.

(28) Christensen, M. A.; Jennum, K.; Abrahamsen, P. B.; Della Pia, E. A.; Lincke, K.; Broman, S. L.; Nygaard, D. B.; Bond, A. D.; Nielsen, M. B. *RSC Adv.* **2012**, *2*, 8243-8249.

(29) Solntsev, K. M.; Poizat, O.; Dong, J.; Rehault, J.; Lou, Y.; Burda, C.; Tolbert, L. M. *J. Phys. Chem. B* **2008**, *112*, 2700-2711.

(30) Kummer, A. D.; Kompa, C.; Niwa, H.; Hirano, T.; Kojima, S.; Michel-Beyerle, M. E. *J. Phys. Chem. B* **2002**, *106*, 7554-7559.

(31) Katoh, R., Suzuki, K.; Furube, A.; Kotani, M; Tokumaru, K. *J. Phys. Chem. C* **2009**, *113*, 2961-2965.

(32) Huang, G.X.; Zhang, G.X.; Wu, Y.S.; Liao, Q.; Fu, H.B.; Zhang, D.Q. *Asian J. Org. Chem.* **2012**, *1*, 352-358.

(33) Shen, X.; Huang, G.; Li, K.; Zhang, G.; Zhang, D. *Sci. China Chem.* **2013**, *9*, 1197-1203.

(34) Ghodbane, A.; Colléaux, J.; Saffon, N.; Mahiou, R.; Galaup, J. P.; Fery-Forgues, S. *ChemPlusChem* **2013**, *78*, 185-191.

(35) Polyakov, I.V.; Grigorenko, B.L.; Epifanovsky, E.M.; Krylov, A.I.; Nemukhin, A.V; *J. Chem. Theory Chem.*, **2010**, *6*, 2377-2387.

(36) Kuhn, H.; Kuhn, C. in *J-Aggregates*, Kobayashi, T. (Ed.), World Scientific, Singapore 1996, pp.1-40.